PNAS

Main Manuscript for

An interstrand DNA crosslink glycosylase aids *Acinetobacter baumannii* pathogenesis

Dillon E. Kunkle[1,2,†], Yujuan Cai[3,†], Brandt F. Eichman[3,4], and Eric P. Skaar[1,2,3]

[1] Department of Pathology, Microbiology, and Immunology, Vanderbilt University Medical Center, Nashville, Tennessee, USA
[2] Vanderbilt Institute for Infection, Immunology, and Inflammation, Vanderbilt University Medical Center, Nashville, Tennessee, USA
[3] Department of Biological Sciences, Vanderbilt University, Nashville, Tennessee, USA
[4] Department of Biochemistry, Vanderbilt University, Nashville, Tennessee, USA
[†] These authors contributed equally to this work

*Corresponding authors: Brandt F. Eichman and Eric P. Skaar

Emails: brandt.eichman@vanderbilt.edu and eric.skaar@vumc.org

Author Contributions: D.E.K and Y.C designed and performed experiments, analyzed data, constructed figures, and wrote the manuscript. B.F.E and E.P.S acquired funding, designed experiments, analyzed data, and edited the manuscript.

Competing Interest Statement: The authors declare no conflict of interest.

Classification: Biological Sciences; Microbiology

Keywords: Bacterial pathogenesis, DNA repair, host-pathogen interactions

This PDF file includes:

Abstract

Maintenance of DNA integrity is essential to all forms of life, including bacteria. DNA damage generated by reaction with genotoxic chemicals result in deleterious mutations, genome instability, and cell death. Interstrand DNA crosslinks (ICLs) are a type of DNA lesion formed by covalent linkage of opposing DNA strands and are particularly toxic as they interfere with replication and transcription. Bacteria have evolved specialized DNA glycosylases that unhook ICLs, thereby initiating their repair. Pathogenic bacteria encounter several genotoxic agents during infection. As such, the loss of DNA repair networks results in virulence attenuation in several bacterial species. In this study we describe AlkX, a DNA glycosylase encoded by the multidrug resistant pathogen *Acinetobacter baumannii*. AlkX exhibits ICL unhooking activity previously described for its *E. coli* homolog, YcaQ. Interrogation of the *in vivo* role of AlkX revealed that the loss of *alkX* impairs *A. baumannii* colonization of the lungs and dissemination to distal tissues, indicating that AlkX protects *A. baumannii* from DNA damaging agents encountered *in vivo*. Moreover, we found that acidic pH, an environment faced during host colonization, results in *A. baumannii* DNA damage, and that a*lkX* is induced by and contributes to defense against acidic conditions. Collectively, these studies reveal new functions for a recently described class of proteins encoded in a broad range of pathogenic bacterial species.

Significance Statement

This work reports a new function for a recently discovered family of DNA glycosylases in the virulence of an important drug resistant bacterial pathogen. Homologs of this protein are encoded within the genomes of several human pathogens. The identification of new classes of proteins that contribute to bacterial pathogenesis is fundamental to the development of novel antimicrobial therapeutics to treat multidrug resistant bacterial infections. Moreover, this family of glycosylase is unique in its ability to initiate repair of interstrand DNA crosslinks. We now report another unique function in mitigating the effects of acidic conditions that occur during infection. Involvement of a DNA repair enzyme in this process provides new avenues of study that will broaden our understanding of bacterial pathogenesis.

Main Text

Introduction

Acinetobacter baumannii is a significant nosocomial pathogen that causes a range of diseases, including respiratory, wound, urinary tract infections, meningitis, endocarditis, and bacteremia (1). This organism accounts for 15-25% of ventilator-associated pneumonias, 10-20% of ICU infections, and is one of the 10 most frequent causes of hospital-acquired bloodstream infections (2). The burden of *A. baumannii* infections is complicated by the rapid evolution of antibiotic resistance in this organism. Several pandrug-resistant *A. baumannii* strains have been isolated from clinics, and *A. baumannii* was recently identified as the fifth leading cause of antimicrobial resistance-associated deaths globally (3-5). In fact, the World Health Organization has identified *A. baumannii* as the number one organism for which the development of new antimicrobials is needed. Collectively, these facts demonstrate the urgent need to identify novel targets for therapeutic intervention against *A. baumannii*. However, *A. baumannii* does not encode for discernable classic virulence determinates, such as toxins, to target for therapeutic intervention. Instead, *A. baumannii* relies on a “persist and resist” virulence strategy, employing a unique capacity to survive in caustic conditions and avoid clearance by the host (6), making it difficult to identify bacterial components to target for therapeutic development.

The maintenance of DNA integrity is an essential process in all living organisms. DNA damage arises from a range of both endogenous and environmental sources. Bacterial pathogens are confronted with a myriad of genotoxic agents at the host-pathogen interface including reactive

oxygen and nitrogen species, acidic pH, antibiotics, and hypochlorous acid (7-11). If left unrepaired, DNA lesions impair fundamental cellular processes, leading to genomic instability and mutations (12). Interstrand DNA crosslinks (ICLs) - formed from covalent adduction of opposing strands of DNA - are a particularly toxic type of DNA damage that inhibit replication and transcription (13, 14). The importance of maintaining genome integrity is illustrated by the numerous DNA repair enzymes in bacterial genomes (15, 16). Among these are DNA glycosylases, which initiate the base excision repair pathway by liberating chemically damaged nucleobases from the DNA backbone (17). Although they typically act on small monoadducts, DNA glycosylases have recently been found to initiate the repair of ICLs (18-20). In addition to their importance in maintaining DNA homeostasis, DNA repair proteins, including DNA glycosylases, are required for virulence in several bacterial pathogens (21-27).

A new family of DNA glycosylases belonging to the HTH_42 superfamily of proteins was identified recently by their proximity to biosynthetic gene clusters (BGCs) in antibiotic-producing bacteria (28-30). These gene clusters encode for the production of a diverse array of genotoxic DNA alkylating agents, including the DNA crosslinker azinomycin B and DNA intercalators trioxacarcin A and hedamycin (31, 32). HTH_42 proteins in these organisms are believed to have evolved as an antitoxin system to protect the host microbe from self-intoxication during bacterial warfare, as HTH_42 proteins show exquisite specificity for DNA lesions produced by the antibiotic generated by the host cell (28, 29, 33). HTH_42 glycosylases are divided into two main clades: AlkZ-like (AZL) and YcaQ-like (YQL) proteins. AZL proteins are encoded within BGCs and serve as self-resistance proteins, while YQL proteins are not associated with a BGC, are produced in the absence of a cognate secondary metabolite, and are often found in non-antibiotic producers (29). Compared to AZL proteins, YQL proteins appear to have a more relaxed substrate specificity and to detoxify an array of lesions, including ICLs derived from the nitrogen mustard mechlorethamine, and thus are hypothesized to serve a generalized role in maintaining genomic stability (19, 29). Importantly, genes encoding for YQL proteins are maintained in the genomes of several important human pathogens, suggesting a role in the maintenance of DNA integrity during infection (19, 28, 29). To date, *E. coli* YcaQ is the only YQL protein to have been characterized (19). There are currently no reports of the role of a YQL family member in a pathogen.

In this study we characterized a YQL protein produced by *A. baumannii*. The *A. baumannii* YQL protects the genome from nitrogen mustard-mediated DNA damage and subsequent toxicity. *In vitro* experiments with purified protein indicate that *A. baumannii* YQL is a DNA glycosylase for both N7-alkylguanine monoadducts and ICLs. The ability of this protein to excise DNA crosslinks led us to name the *A. baumannii* YQL protein AlkX. Exploration of the role of AlkX in *A. baumannii* virulence revealed that *alkX* is induced within the host during pneumonic infection and contributes to *A. baumannii* colonization of the lung and dissemination to distal tissues. These findings suggest that AlkX protects *A. baumannii* from a genotoxic stress encountered within the host. Consistent with this, we found that acidic pH, a stressor that *A. baumannii* faces within the host while interacting with immune cells and commensal bacteria, results in DNA damage and induction of *alkX.* Further, the loss of AlkX results in reduced fitness under acidic conditions. Collectively, these findings implicate a new class of DNA repair proteins in bacterial pathogenesis and reveal a previously unappreciated function for YQL proteins in the response to a stress condition that *A. baumannii* encounters during host colonization. These findings suggest that HTH_42 proteins in non-antibiotic producing bacteria have evolved to serve specialized functions that are specific to the lifestyle of their host organism, which may represent an attractive novel target for the development of antimicrobials.

Results

A. baumannii encodes an HTH_42 DNA glycosylase that protects against interstrand DNA crosslinks

Analysis of the *A. baumannii* 17978VU genome revealed that *A. baumannii* encodes an HTH_42 protein in locus *AXC60_11575.* The *A. baumannii* YQL protein has a high level of homology—32% sequence identity and 49% similarity—to the *E. coli* HTH_42 protein, YcaQ. Based on this homology and experimental results described below, we have renamed this *A. baumannii* gene *alkX.* We hypothesized that *A. baumannii* AlkX serves a similar function as YcaQ and therefore *alkX* may be regulated in response to treatment with genotoxic agents. Expression of *alkX* was strongly induced following treatment with mechlorethamine (Fig. 1A), while exposure to other DNA damaging agents, including other alkylators, did not impact expression (Fig. S1A). To determine if AlkX protects *A. baumannii* from the antibacterial effects of mechlorethamine, we generated an *alkX* deletion strain. Loss of *alkX* resulted in increased susceptibility to mechlorethamine (Fig. 1B). Consistent with expression data, this phenotype was specific to mechlorethamine as treatment with other genotoxic compounds did not result in differential growth between Δ*alkX* and WT (Fig. S1 B-D). To determine if this phenotype is specifically due to the loss of AlkX, *alkX* was expressed *in trans* in the Δ*alkX* genetic background, fully restoring growth to WT levels in the presence of mechlorethamine (Fig. 1C & S2). These data collectively indicate that AlkX protects *A. baumannii* from the genotoxic effects of mechlorethamine.

Previous studies identified a highly conserved QΦD motif (where Φ is a hydrophobic residue) in YQL proteins that is required for ICL unhooking activity, in which alanine substitution of either conserved glutamine or aspartate residue rendered the protein functionally inactive (19, 29, 34). Therefore, to assess if the AlkX-dependent protection from mechlorethamine-mediated growth repression is dependent on the catalytic activity of AlkX, alanine substitutions were made in these conserved residues (Q39A and D41A). Expression of the Q39A and D41A mutant alleles of *alkX* in the Δ*alkX* mutant background revealed that disruption of the catalytic activity significantly reduced the capacity of AlkX to protect against mechlorethamine treatment (Fig. 1C & S2), suggesting that AlkX protects against DNA alkylation through a conserved unhooking of DNA adducts. To determine if AlkX is sufficient for protection from mechlorethamine-mediated killing we leveraged the finding that the non-pathogenic *Acinetobacter* species *A. baylyi* does not encode an *alkX* homologue (Fig. S3). Compared with *A. baumannii*, *A. baylyi* showed more susceptibility to mechlorethamine (Fig. 1B & 1D). Expression of *alkX* in *A. baylyi* resulted in increased cellular survival during mechlorethamine treatment (Fig. 1D). Collectively, these data indicate that *A. baumannii* produces a YQL HTH_42 family protein that is necessary and sufficient for the detoxification of mechlorethamine-mediated DNA damage.

AlkX retains conserved DNA unhooking activity and participates in maintenance of DNA integrity

To determine if AlkX exhibits N7-alkylguanine DNA glycosylase activity consistent with its homologues AlkZ (34) and YcaQ (19), purified AlkX was incubated with a 5′-Cy5-labeled oligodeoxynucleotide containing an N7-methyldeoxyguanosine (d7mG) monoadduct followed by treatment with hydroxide to nick any resulting apurinic/apyrimidinic (AP, or abasic) sites (Fig. S4). In this assay, AlkX exhibited base excision activity, hydrolyzing ~80% d7mG after 5 minutes of incubation (Fig. 2A&B). We confirmed separately by heat treatment that this substrate contains 88% hydrolyzable d7mG. The requirement of the Q39 and D41 residues in the catalytic activity was confirmed by the observation that alanine substitutions of either residue resulted in near complete abrogation of base excision activity. After one hour, the Q39A mutant hydrolyzed 3% d7mG and D41A displayed no observable activity (Fig. 2A&B).

Next, the ability of AlkX to unhook mechlorethamine-derived ICLs was assessed. Incubation of mechlorethamine with a DNA containing a d(GTC)/d(GAC) sequence produces a 5-atom nitrogen mustard (NM) ICL (Fig. 2C). The substrate contained a 5′-FAM dye on one strand and a 5′-Cy5 on the other so that excision of either strand could be followed (Fig. 2C). AlkX exhibited rapid unhooking of the NM-ICL, with almost all of the substrate unhooked after 5 minutes (Fig. 2D,E & S5). The Q39A and D41A substitutions impaired activity, but not to the level reached for the d7mG-DNA substrate. After one hour, Q39A and D41A mutants unhooked 53% and 45% of the

NM-ICL, respectively, compared to 17% for a no-enzyme control (Fig. 2D,E & S5). ICL unhooking generated an appreciable amount of monoadduct that was not further hydrolyzed to an AP site (Fig. 2F), consistent with the lack of hydrolysis of d7mG monoadduct by the mutants.

These findings indicate that the loss of AlkX catalytic activity results in increased susceptibility to mechlorethamine-mediated growth repression, and that purified AlkX exhibits conserved ICL unhooking activity *in vitro* that is also dependent on catalytic activity. The impact of the loss of *alkX* on damage to the *A. baumannii* chromosome was then assessed. To elucidate this, whole genomic DNA (gDNA) was purified from WT and Δ*alkX A. baumannii* in the presence or absence of DNA alkylating agents. Purified gDNA was treated with BAL-31, a nuclease that cleaves DNA at sites of damage including nicks, single-stranded regions, and AP sites (35). Consistent with this, treatment of *A. baumannii* with either DNA alkylating agent mechlorethamine or mitomycin C resulted in increased BAL-31 digestion of gDNA (Figs. 2G,H & S6). The loss of *alkX* resulted in increased DNA damage when cells were treated with mechlorethamine, compared to WT cells (Fig. 2G,H). Further, this phenotype was fully complemented when WT *alkX* was supplied *in trans* in the Δ*alkX* background. The expression of catalytically inactive forms of AlkX were unable to fully complement this phenotype (Fig. 2G,H). Consistent with the growth and expression data, treatment of *A. baumannii* cells with mitomycin C did not result in increased DNA damage in the absence of AlkX (Fig. S6), indicating that the observed phenotype is specific to DNA alkylation induced by mechlorethamine. Collectively, these results indicate that AlkX is a DNA glycosylase that unhooks and protects the *A. baumannii* genome from guanine N7-substituted ICLs.

AlkX functions in *A. baumannii* virulence

Genes encoding for proteins from the YQL clade of HTH_42 proteins are maintained in the genomes of several human pathogens (19, 28, 29), yet there are no reports of a function for these enzymes in bacterial virulence. Only pathogenic *Acinetobacter* species encode for *alkX* homologues (Fig. S3). Additionally, the sequences and key catalytic residues of *alkX* are highly conserved in the sequenced genomes of *A. baumannii* clinical isolates that have been isolated across several years and numerous countries (Fig. S7). Combined, these observations led to the hypothesis that *alkX* is maintained in pathogenic *A. baumannii* strains because it confers a selective advantage during infection. To test this hypothesis, a mouse model of bacterial pneumonia was used. WT and Δ*alkX A. baumannii* strains were used to intranasally infect female C57BL/6J mice. At 36 hours post-infection (hpi), the lungs, hearts, livers, spleens, and kidneys were harvested and bacterial burdens in each organ were enumerated. These experiments revealed that the loss of *alkX* resulted in a reduced capacity to colonize the mouse lung, and to disseminate to the heart and kidneys (Fig. 3 A-E), indicating that AlkX likely contributes to *A. baumannii* DNA stability within the host.

During infection bacterial pathogens face several assaults that result in DNA damage (36-38). Given our findings that AlkX participates in *A. baumannii* virulence we sought to assess if *A. baumannii* induces DNA repair pathways within the host, including *alkX.* To this end, mice were infected with WT *A. baumannii* strains harboring $P_{alkX,}$ P_{uvrA}, and P_{recA} luciferase reporter fusion constructs and bioluminescent imaging was performed to measure *in vivo* bacterial gene expression. *uvrA* and *recA* are rapidly induced in response to several DNA damaging conditions and thus serve as markers for genotoxic stress (39, 40). Luciferase reporter plasmids were well maintained in the lungs of mice, and maintenance of individual plasmids did not impact bacterial colonization (Figs. S8). Consistent with previous findings indicating that genes encoding for DNA repair proteins RecF and RecO are induced by *A. baumannii* during colonization of the mouse lung (41), both *uvrA* and *recA* genes were expressed in the host during infection, both at the initial infection site of the lung and in distal tissues (Figs. 3F&G). In keeping with the colonization data, expression of *alkX* was also significantly induced in the host. Collectively, these data indicate that *A. baumannii* encounters genotoxic stress during pneumonic infection, including stressors that result in the induction of *alkX*.

AlkX participates in *A. baumannii* acid tolerance

A. baumannii induces *alkX* during colonization of the host, and loss of *alkX* results in a reduced capacity for *A. baumannii* to colonize the mouse lung and to disseminate to distal organs. These results suggest that AlkX protects *A. baumannii* from assaults encountered during infection. Therefore, we sought to determine the *in vivo* relevant signal to which *alkX* responds. *E. coli* YcaQ serves as a secondary pathway to UvrA-mediated repair of nitrogen mustard-induced DNA damage (19), and *alkX* is specifically induced by, and protects from, mechlorethamine toxicity (Fig. 1). These results led us to hypothesize that AlkX and UvrA respond to, and are important during, similar stress conditions. UvrA functions in the response to DNA damage induced by acidic pH in several organisms (42-44). Low pH is a caustic environment that pulmonary pathogens, like *A. baumannii*, encounter in the lung environment due to interactions with commensal bacteria and host immune cells (45, 46). These facts led us to explore if AlkX also plays a role under acidic growth conditions.

First, we determined that exposure to an acidic environment induced a pH-dependent increase in damage to *A. baumannii* gDNA (Fig. 4A,B & S9A), and consistent with previous reports in other organisms (8, 47), acidic conditions resulted in induction of *uvrA* expression (Fig. 4C). These results indicate that acidic environments induce genotoxic stress in *A. baumannii*. Low pH appeared to induce broad DNA damage in *A. baumannii*, as *recA* expression was also induced under these conditions (Fig. S9B). Consistent with this, *alkX* expression was induced when *A. baumannii* was cultured under acidic conditions (Fig. 4D). Thus, we explored if AlkX functioned in *A. baumannii* survival in an acidic environment. The loss of *alkX* resulted in decreased fitness, relative to WT, when strains were grown at pH 5.25, and this phenotype was fully complemented to WT levels when expressing *alkX in trans* in the Δ*alkX* background (Fig. 4E). These results indicate that the loss of AlkX was specifically responsible for the reduced growth at acidic pH. To determine if the loss of *alkX* resulted in increased genotoxic stress under these conditions, *uvrA* expression was measured in both the WT and Δ*alkX* mutant backgrounds when cultured at neutral and acidic pH. These experiments revealed that at acidic pH *uvrA* expression is induced in a Δ*alkX* background relative to WT cells (Fig. 4F). However, the loss of *alkX* did not result in differential expression of *recA* under these conditions (Fig. S9B). These observations indicate that at low pH the loss of AlkX results in increased genotoxic stress sensed by the cell, and specifically increases *uvrA* expression. These findings collectively suggest that *A. baumannii* may induce *alkX* expression in acidic environments as an adaptive response for the maintenance of genomic integrity.

Discussion

Expression of *alkX* was induced upon exposure to mechlorethamine, but not to other DNA damaging agents (Fig. 1A & S1A). This is in contrast to *E. coli ycaQ*, which is not differentially regulated in response to mechlorethamine (19). This difference is likely due to the fact that *ycaQ* is encoded within an operon downstream of several essential genes under the regulation of a constitutive σ^{70}-dependent promoter (19), while *alkX* is encoded outside of an operon and maintains its own promoter (Fig. S3). These findings suggest that AlkX has evolved to serve a specialized function specific to the lifestyle of *A. baumannii* and may contribute to the “persist and resist” virulence strategy utilized by *A. baumannii* (6). This hypothesis is supported by the recent finding that loss of *alkX* is detrimental for *A. baumannii* to survive desiccation, an environment known to induce DNA damage (48, 49). Desiccation resistance is an important adaptation that promotes *A. baumannii* survival on hospital surfaces and has been correlated with outbreak strains of *A. baumannii* (50, 51). Thus, evolution of specialized systems to maintain genomic stability in these environments may aid in the nosocomial spread of the pathogen. These observations suggest that in the absence of host cell antibiotic production, YQL proteins have evolved to serve specialized functions to benefit the specific lifestyles of pathogenic organisms. Evolution of DNA repair systems to accommodate specific environments has been recorded in another pathogenic *Acinetobacter* species, indicating that DNA repair systems are under environment-specific selection (52). Future

investigations of other YQL proteins and their genomic neighbors may shed light on the specialized function of these proteins in their native organisms.

Low pH is an assault that respiratory pathogens face during infection both within the lung environment and during interaction with host immune cells (45, 46). The *A. baumannii* acid response has been linked to important pathogenic phenotypes including resistance to last-resort antibiotics, immune cell evasion, and the avoidance of clearance by the host. This suggests that acid resistance may be a key strategy that enables *A. baumannii* to persist during infection, which leads to enhanced *A. baumannii*-induced mortality (53-57). Consistent with previous reports, we found that *A. baumannii* experiences genomic stress when it encounters acidic pH (8, 47), and that DNA repair genes *uvrA, recA,* and *alkX* were induced both by acidic pH and during host infection. These observations coupled with the finding that the loss of *alkX* results in reduced capacity of *A. baumannii* to persist within the host indicates that acid-induced DNA damage may be an underappreciated mechanism for the clearance of bacterial infections. The observation that the loss of *alkX* results in both increased acid susceptibility and reduced *in vivo* fitness suggests that the role of AlkX in survival within acidic environments may be the mechanism responsible for the observed virulence defect.

AlkX functions in ICL repair, a conserved function with *E. coli* YcaQ, the only other characterized YQL family member (19). In both organisms this activity results in detoxification of nitrogen mustard-induced DNA crosslinks. Given that nitrogen mustards are not ubiquitous in the environment it is unlikely that genes that encode for YQL family members evolved in bacteria to detoxify these DNA lesions. Although it is believed that several native compounds are capable of intercalating into DNA, their identity remains elusive (58). Here, we have found that AlkX not only aids in defense against nitrogen mustard-induced toxicity, but also against acid stress, a newly reported role for YQL family proteins. Although the mechanism of the protection against acid stress remains unknown, it is possible that acidic conditions result in the production or chemical alteration of endogenous metabolites capable of DNA intercalation. Consistent with this hypothesis, we and others have found that acidic pH results in increased DNA damage (Fig. 4A&B). However, the exact nature of these aberrations remains unexplored (8, 47). Whether this is a conserved function in other YQL family members encoded for by other pathogenic organisms requires further investigation.

Targeting the ability of pathogens to maintain genomic stability has proven to be a reliable strategy for the development of antimicrobials (59). Our finding that the loss of *alkX* resulted in a reduced capacity to colonize the mouse lung and disseminate to distal tissues, coupled with the fact that humans do not encode for this protein, suggest that these proteins may represent a target for novel antimicrobial therapies. In support of this, inhibitors that target both eukaryotic and prokaryotic DNA glycosylases have been developed (60, 61). It has been suggested that alone, or in combination with genotoxic agents, bacterial glycosylase inhibitors may be an effective therapeutic strategy to combat antimicrobial resistance (60). Several classes of antibiotics have been shown to result in genomic instability in bacterial cells (62). Therefore, the therapeutic targeting of novel microbial pathways that maintain DNA integrity may potentiate existing antimicrobials in otherwise resistant pathogens.

Materials and Methods

Animal experiments

Mouse experiments were performed using female 8–12 week old C57BL/6J mice supplied by Jackson Laboratories. Animals were maintained at the Vanderbilt University Medical Center (VUMC) Animal Facilities, with a 12 h light-dark cycle and food and water provided ad libitum. For experimental endpoints, animals were humanely euthanized. All animal experiments were

approved and performed in compliance with the Institutional Animal Care and Use Committee (IACUC) of Vanderbilt University (protocol number M1900043-00) and conform to policies and guidelines established by VUMC, the Animal Welfare Act, the National Institutes of Health, and the American Veterinary Medical Association.

Bacterial strains and growth conditions

Bacterial strains used in this study are listed in Table S1. Bacteria were cultured in lysogeny broth (LB) or on LB with 1.5% w/v agar (LBA). For the purposes of plasmid maintenance and screening for mutational insertion, antibiotics were added at the following concentrations: carbenicillin, 75 µg/mL; chloramphenicol, 15 µg/mL; kanamycin, 30 µg/mL (*E. coli*), and 40 µg/mL (*A. baumannii*); tetracycline, 5 µg/mL (*E. coli*), and 10 µg/mL (*A. baumannii*). For experiments with LB buffered at specific pH either 100 mM HEPES was added to LB to buffer at pH 7, and 100mM MES was added to buffer at all acidic pH values.

Cloning and genetic manipulation

All plasmids and primers used in this study are listed in Table S1. Prior to use all cloned vectors were confirmed by Sanger sequencing. P_{alkX}, P_{recA}, and P_{uvrA} luciferase transcriptional reporter plasmids were generated by amplifying target gene promoters using *A. baumannii* genomic DNA as a PCR template and cloning them into a SacI and BamHI digested pMU368(tet)-lux vector using HiFi Assembly (NEB) following the manufacturer's protocol. The *alkX* expression vector was generated by amplifying the *alkX* locus, including the native promoter using *A. baumannii* genomic DNA as a PCR template and cloning it into a SalI and BamHI digested pWH1266 vector using HiFi Assembly. *alkXQ39A* and *alkXD41A* mutant allele expression constructs were generated by site-directed mutagenesis as follows. The pWH1266-*alkX* vector was amplified in a PCR reaction with primers encoding the indicated point mutants. The resulting PCR product was DpnI digested and transformed into *E. coli.* Plasmids harboring the desired mutations were screened by Sanger sequencing. AlkX purification vectors were constructed as follows. The *alkX* gene was subcloned into pBG102 vector using gene-specific primers to produce the protein with N-terminal His_6 and SUMO tags. Mutations were introduced using the Q5 Site-Directed Mutagenesis kit (New England Biolabs). For generation of the Δ*alkX* construct 1,000 bp of DNA in both the 5′ and 3′ flanking regions surrounding the *alkX* gene were amplified using *A. baumannii* genomic DNA as a PCR template. The kanamycin resistance gene *aphA* was amplified by PCR from the vector pUCK1. These products were cloned into a XbaI and BamHI digested pFLp2 vector using HiFi Assembly. Using the resulting construct the Δ*alkX* mutant was created via allelic exchange as follows. The construct was introduced into WT *A. baumannii* by tri-parental conjugation using an HB101 *E. coli* strain containing the helper plasmid pRK2013 on LBA for ~18 hr. Matings were plated onto LBA containing carbenicillin 75 µg/mL and chloramphenicol 15 µg/mL to select for strains containing the integrated allelic exchange plasmid. Strains were then plated onto LBA containing 10% sucrose to select for clones that had resolved the integrated plasmid and resulting sucrose-resistant colonies. Resulting sucrose-resistant colonies were patched onto LBA supplemented with kanamycin 40 µg/mL. Deletion of *alkX* was confirmed first by PCR with primers outside of the inserted *aphA* construct, followed by whole-genome sequencing (Seq-center).

Bacterial growth curves

Overnight cultures of indicated strains were started from single colonies in LB broth, with antibiotics when appropriate. The following day overnight cultures were back-diluted into fresh LB media 1:50, and allowed to grow with shaking at 37 °C for 1 hr. Back diluted cultures were used to inoculate the wells of 96 well microtiter plates 1:100 with indicated media. Plates were cultured with continuous shaking at 37 °C for 18 hr and OD_{600} was recorded every 60 min.

Luciferase transcriptional reporter assays

Overnight cultures of indicated strains harboring indicated luciferase transcriptional reporter plasmids were started from single colonies in LB broth with the addition of tetracycline. The following day overnight cultures were back-diluted into fresh LB media with tetracycline 1:50, and allowed to grow with shaking at 37 °C for 1 hr. Back diluted cultures were used to inoculate the wells of black clear bottom 96 well microtiter plates 1:100 with indicated media containing tetracycline. Plates were cultured with continuous shaking at 37 °C for 10 hr and total luciferase and OD_{600} were recorded every 60 min. Data are reported as luciferase divided by the OD_{600} of the culture.

Protein purification

WT and mutant AlkX proteins were expressed in *E. coli* Tuner (DE3) cells in LB media in the presence of 30 μg/mL kanamycin. Expression was induced by treatment with 0.1 mM IPTG (isopropyl-β-D-thiogalactopyranoside) when the OD_{600} of the culture reached 0.6. After growing for 16 hr at 16 °C, the cells were harvested, homogenized in 50 mM Tris (pH 8.0), 500 mM NaCl, 1 mM Tris (2-carboxyethyl) phosphine (TCEP), 1 mM phenylmethylsulfonyl fluoride (PMSF), 25 mM imidazole, 10% glycerol, and lysed by sonication. Cell debris was removed by centrifugation at 21,000 rpm for 30 min at 4 °C. The supernatant was loaded onto an Ni-NTA affinity column (Cytiva), and the His-tagged protein was eluted with buffer B (50 mM Tris (pH 8.0), 500 mM NaCl, 250 mM imidazole, 10% glycerol). Protein fractions were pooled and supplemented with 0.1 mM EDTA and 1 mM TCEP before incubation with 1 mg Rhinovirus 3C (PreScission) protease at 4 °C overnight. The cleaved protein was diluted 5-fold with buffer C (50 mM Tris (pH 8.0), 10% glycerol, 0.1 mM EDTA, 1 mM TCEP) and purified on a heparin sepharose column (Cytiva) with a 0–1 M NaCl/buffer C linear gradient. Fractions were pooled and repassed over the Ni-NTA affinity column. The flow-through was concentrated using a 10-kDa MWCO Amicon Ultra filter (Millipore). The concentrated protein was then purified over a Superdex 200 column (Cytiva) in 25 mM Tris (pH 8.0), 150 mM NaCl, 5% glycerol, 0.1 mM EDTA, 1 mM TCEP. The peak fractions were collected and concentrated to 5 mg/mL and flash-frozen in liquid nitrogen and stored at -80 °C.

Base excision assays

The d7mG (63, 64) and NM-ICL DNA substrates were prepared as described previously using oligodeoxynucleotides in Table S1 (19). ICL_top and ICL_bottom were annealed at 200 μM in annealing buffer (10 mM MES pH 6.5, 40 mM NaCl). NM-ICL DNA substrates were generated by reaction of 100 μM annealed duplex with 300 μM mechlorethamine hydrochloride in 40 mM sodium cacodylate buffer (pH 7.0) at 37 °C for 3 hr (65). Products were desalted using Microspin G-25 columns and purified on a 15% acrylamide/8M urea gel in TBE buffer.

In each glycosylase reaction, 1 μM enzyme was incubated with 50 nM DNA substrate in glycosylase buffer (50 mM HEPES pH 8.5, 100 mM KCl, 10 mM EDTA, and 10% glycerol) at 25 °C. At each time point, a 4-μL aliquot was removed and added to 1 μL of 1 M NaOH. For the d7mG excision assay, the samples were heated at 70 °C for 2 min followed by addition of 5 μL denaturing loading buffer (5 mM EDTA pH 8.0, 80% formamide, 1 mg/ml blue dextran) and heated at 70 °C for 5 min. For the NM-ICL excision assay, samples were heated at 55 °C for 2 min followed by adding 5 μL of denaturing loading buffer and heating at 55 °C for 5 min to avoid spontaneous depurination at high temperature. All samples were electrophoresed on a 20% acrylamide/8 M urea denaturing gel at 40 W for 1 hr (for d7mG substrates) or 2 hr (for NM-ICL substrates) in 0.5× TBE buffer. Gels were imaged on a Typhoon RGB scanner (Cytiva). Bands were quantified with ImageQuant (Cytiva). All excision assays were performed in triplicate.

Whole-cell DNA damage quantification

Experiments were carried out according to (8) with few modifications. Overnight bacterial cultures of the indicated strains were used to inoculate fresh LB media 1:1000 and cultured at 37 °C with shaking. At mid-log phase cultures were left untreated or treated with 50 μM mechlorethamine or

50 μM mitomycin C. For acid-induced damage of DNA cultures were centrifuged, washed with sterile PBS, and resuspended in LB media at the indicated pH values. One hr post treatment 1 mL of cultures were harvested, and total gDNA was isolated using a DNeasy (Qiagen) kit according to the manufacturer's protocol. One μg of gDNA was used in BAL-31 digestion reactions with 0.2 U of BAL-31 in 20 μL of nuclease buffer. Digestions were carried out for 30 min at 30 °C, then heated for 10 min at 75 °C. The reactions were electrophoresed on a 0.8% agarose gel and visualized using a BioRad Chemidoc imager. To quantify DNA damage across several biological replicates, Image Lab software (Bio-Rad) was used to quantify the density of the entire lane, including the undigested gDNA band, and the density of the gDNA band alone were recorded. % uncut DNA was calculated by dividing the intensity of the undigested gDNA band by the intensity of the entire lane.

Mouse infections and *in vivo* imaging

A. baumannii overnight cultures were diluted 1:1000 in fresh LB for 3.5 hr when cultures were harvested, washed twice in sterile PBS, and suspended in sterile PBS to ~1x10^{10} CFU/mL and serially diluted and spot-plated to confirm equivalent bacterial concentrations between strains and experiments. Prior to infections, mice were anesthetized by intraperitoneal injection of 2,2,2 tribromoethanol diluted in sterile PBS. Anesthetized mice were infected intranasally with a 40 μL volume of the bacterial inoculum (9.6 x 10^7 - 6.0 x 10^8 cfu). Infections were allowed to proceed for 36 hr, during which time mouse weight and survival was monitored. Mice were euthanized by forced CO_2 inhalation followed by cervical dislocation, and lungs, hearts, livers, spleens, and kidneys were sterilely harvested. Organs were homogenized and serial dilutions of homogenized tissues were spot plated onto LB agar for enumeration.

WT *A. baumannii* strains harboring P_{uvrA}, P_{recA}, and P_{alkX} transcriptional reporter fusion plasmids cultured in 10 μg/mL tetracycline were prepared for and used in mouse infections as above. At time of infection Nair was applied to the abdomen and fur wiped away. At 36 hpi mice were anesthetized via inhalation of isoflurane and imaged for bioluminescence with a PerkinElmer IVIS Spectrum at the VUMC Institute of Imaging Science Center for Small Animal Imaging. Images were analyzed with the Living Image software. ROIs were drawn over each animal and total photon flux was determined, and background luminescence subtracted. Fold change for individual genes was calculated by dividing total luminescence of strains infected with WT *A. baumannii* harboring an empty vector control. Percent plasmid retention and CFU's were determined by serial dilutions of lung homogenates onto both LB plates and LB plates containing 10 μg/mL tetracycline and bacterial burdens enumerated. % plasmid retention represents the % of CFU's that were tet^R over the total CFU's.

Quantification, statistical analysis, and software

Raw data were recorded in Microsoft Excel and imported into GraphPad Prism 10 for statistical analysis. *In vivo* images were captured and analyzed using PerkinElmer Living Image software. Figures were generated in GraphPad Prism 10 and designed in Canvas X. Data were analyzed as indicated in figure legends. Asterisks indicate the statistical significance: * $p < 0.05$, ** $p < 0.01$, *** $p < 0.001$, **** $p < 0.0001$, ns = not significant. N values, definitions of center, and dispersion and precision measurements for each experiment are reported in the figure legends.

Acknowledgments

This work was supported by grants from the National Institutes of Health (R01AI101171 and R01AI150701 to E.P.S.) and the National Science Foundation (MCB-1928918 to B.F.E.).

References

1. A. Y. Peleg, H. Seifert, D. L. Paterson, *Acinetobacter baumannii*: emergence of a successful pathogen. *Clin Microbiol Rev* **21**, 538-582 (2008).
2. J. L. Vincent *et al.*, International study of the prevalence and outcomes of infection in intensive care units. *Jama* **302**, 2323-2329 (2009).
3. J. M. Rolain *et al.*, Real-time sequencing to decipher the molecular mechanism of resistance of a clinical pan-drug-resistant *Acinetobacter baumannii* isolate from Marseille, France. *Antimicrob Agents Chemother* **57**, 592-596 (2013).
4. T. Wongsuk, S. Boonsilp, A. Homkaew, K. Thananon, W. Oonanant, Whole genome sequence of pan drug-resistant clinical isolate of *Acinetobacter baumannii* ST1890. *PLoS One* **17**, e0264374 (2022).
5. Anonymous, Global burden of bacterial antimicrobial resistance in 2019: a systematic analysis. *Lancet* **399**, 629-655 (2022).
6. C. M. Harding, S. W. Hennon, M. F. Feldman, Uncovering the mechanisms of *Acinetobacter baumannii* virulence. *Nat Rev Microbiol* **16**, 91-102 (2018).
7. E. Schlosser-Silverman, M. Elgrably-Weiss, I. Rosenshine, R. Kohen, S. Altuvia, Characterization of *Escherichia coli* DNA lesions generated within J774 macrophages. *J Bacteriol* **182**, 5225-5230 (2000).
8. K. C. Jeong, K. F. Hung, D. J. Baumler, J. J. Byrd, C. W. Kaspar, Acid stress damage of DNA is prevented by Dps binding in *Escherichia coli* O157:H7. *BMC Microbiol* **8**, 181 (2008).
9. A. Ulfig, L. I. Leichert, The effects of neutrophil-generated hypochlorous acid and other hypohalous acids on host and pathogens. *Cell Mol Life Sci* **78**, 385-414 (2021).
10. Z. Baharoglu, D. Mazel, *Vibrio cholerae* triggers SOS and mutagenesis in response to a wide range of antibiotics: a route towards multiresistance. *Antimicrob Agents Chemother* **55**, 2438-2441 (2011).
11. S. A. Weitzman, T. P. Stossel, Mutation caused by human phagocytes. *Science* **212**, 546-547 (1981).
12. S. P. Jackson, J. Bartek, The DNA-damage response in human biology and disease. *Nature* **461**, 1071-1078 (2009).
13. K. S. Gates, An overview of chemical processes that damage cellular DNA: spontaneous hydrolysis, alkylation, and reactions with radicals. *Chem Res Toxicol* **22**, 1747-1760 (2009).
14. A. J. Deans, S. C. West, DNA interstrand crosslink repair and cancer. *Nat Rev Cancer* **11**, 467-480 (2011).
15. K. J. Wozniak, L. A. Simmons, Bacterial DNA excision repair pathways. *Nat Rev Microbiol* **20**, 465-477 (2022).
16. D. B. Wigley, Bacterial DNA repair: recent insights into the mechanism of RecBCD, AddAB and AdnAB. *Nat Rev Microbiol* **11**, 9-13 (2013).
17. A. L. Jacobs, P. Schär, DNA glycosylases: in DNA repair and beyond. *Chromosoma* **121**, 1-20 (2012).
18. D. R. Semlow, J. Zhang, M. Budzowska, A. C. Drohat, J. C. Walter, Replication-Dependent Unhooking of DNA Interstrand Cross-Links by the NEIL3 Glycosylase. *Cell* **167**, 498-511.e414 (2016).
19. N. P. Bradley, L. A. Washburn, P. P. Christov, C. M. H. Watanabe, B. F. Eichman, *Escherichia coli* YcaQ is a DNA glycosylase that unhooks DNA interstrand crosslinks. *Nucleic Acids Res* **48**, 7005-7017 (2020).
20. E. A. Mullins, A. A. Rodriguez, N. P. Bradley, B. F. Eichman, Emerging Roles of DNA Glycosylases and the Base Excision Repair Pathway. *Trends Biochem Sci* **44**, 765-781 (2019).
21. N. A. Buchmeier, C. J. Lipps, M. Y. So, F. Heffron, Recombination-deficient mutants of Salmonella typhimurium are avirulent and sensitive to the oxidative burst of macrophages. *Mol Microbiol* **7**, 933-936 (1993).
22. K. Poncin *et al.*, Occurrence and repair of alkylating stress in the intracellular pathogen *Brucella abortus*. *Nat Commun* **10**, 4847 (2019).

23. T. Zhang, D. Bae, C. Wang, *Listeria monocytogenes* DNA Glycosylase AdlP Affects Flagellar Motility, Biofilm Formation, Virulence, and Stress Responses. *Appl Environ Microbiol* **82**, 5144-5152 (2016).
24. J. Venkatesh, P. Kumar, P. S. Krishna, R. Manjunath, U. Varshney, Importance of uracil DNA glycosylase in *Pseudomonas aeruginosa* and *Mycobacterium smegmatis*, G+C-rich bacteria, in mutation prevention, tolerance to acidified nitrite, and endurance in mouse macrophages. *J Biol Chem* **278**, 24350-24358 (2003).
25. A. R. Richardson *et al.*, The Base Excision Repair system of *Salmonella enterica* erovar typhimurium counteracts DNA damage by host nitric oxide. *PLoS Pathog* **5**, e1000451 (2009).
26. E. Guillemet *et al.*, The bacterial DNA repair protein Mfd confers resistance to the host nitrogen immune response. *Sci Rep* **6**, 29349 (2016).
27. R. Eutsey, G. Wang, R. J. Maier, Role of a MutY DNA glycosylase in combating oxidative DNA damage in *Helicobacter pylori*. *DNA Repair (Amst)* **6**, 19-26 (2007).
28. S. Wang *et al.*, Characterization of a novel DNA glycosylase from *S. sahachiro*i involved in the reduction and repair of azinomycin B induced DNA damage. *Nucleic Acids Res* **44**, 187-197 (2016).
29. N. P. Bradley, K. L. Wahl, J. L. Steenwyk, A. Rokas, B. F. Eichman, Resistance-Guided Mining of Bacterial Genotoxins Defines a Family of DNA Glycosylases. *mBio* **13**, e0329721 (2022).
30. Q. Zhao *et al.*, Characterization of the azinomycin B biosynthetic gene cluster revealing a different iterative type I polyketide synthase for naphthoate biosynthesis. *Chem Biol* **15**, 693-705 (2008).
31. M. Zhang *et al.*, Biosynthesis of trioxacarcin revealing a different starter unit and complex tailoring steps for type II polyketide synthase. *Chem Sci* **6**, 3440-3447 (2015).
32. T. Bililign, C. G. Hyun, J. S. Williams, A. M. Czisny, J. S. Thorson, The hedamycin locus implicates a novel aromatic PKS priming mechanism. *Chem Biol* **11**, 959-969 (2004).
33. X. Chen *et al.*, Base excision repair system targeting DNA adducts of trioxacarcin/LL-D49194 antibiotics for self-resistance. *Nucleic Acids Res* **50**, 2417-2430 (2022).
34. E. A. Mullins, G. M. Warren, N. P. Bradley, B. F. Eichman, Structure of a DNA glycosylase that unhooks interstrand cross-links. *Proc Natl Acad Sci U S A* **114**, 4400-4405 (2017).
35. C. F. Wei, R. J. Legerski, G. A. Alianell, D. L. Robberson, H. B. Gray, Jr., A single apurinic site can elicit BAL 31 nuclease-catalyzed cleavage in duplex DNA. *Biochim Biophys Acta* **782**, 408-414 (1984).
36. E. J. O'Rourke *et al.*, Pathogen DNA as target for host-generated oxidative stress: role for repair of bacterial DNA damage in *Helicobacter pylori* colonization. *Proc Natl Acad Sci U S A* **100**, 2789-2794 (2003).
37. L. Fialkow, Y. Wang, G. P. Downey, Reactive oxygen and nitrogen species as signaling molecules regulating neutrophil function. *Free Radic Biol Med* **42**, 153-164 (2007).
38. S. van der Veen, C. M. Tang, The BER necessities: the repair of DNA damage in human-adapted bacterial pathogens. *Nature Reviews Microbiology* **13**, 83-94 (2015).
39. M. D. Norton, A. J. Spilkia, V. G. Godoy, Antibiotic resistance acquired through a DNA damage-inducible response in *Acinetobacter baumannii*. *J Bacteriol* **195**, 1335-1345 (2013).
40. J. Courcelle, A. Khodursky, B. Peter, P. O. Brown, P. C. Hanawalt, Comparative gene expression profiles following UV exposure in wild-type and SOS-deficient *Escherichia coli*. *Genetics* **158**, 41-64 (2001).
41. G. L. Murray *et al.*, Global Gene Expression Profile of *Acinetobacter baumannii* During Bacteremia. *J Infect Dis* **215**, S52-s57 (2017).
42. M. N. Hanna, R. J. Ferguson, Y. H. Li, D. G. Cvitkovitch, *uvrA* is an acid-inducible gene involved in the adaptive response to low pH in *Streptococcus mutans*. *J Bacteriol* **183**, 5964-5973 (2001).
43. T. K. Moghaddam, J. Zhang, G. Du, UvrA expression of *Lactococcus lactis* NZ9000 improve multiple stresses tolerance and fermentation of lactic acid against salt stress. *J Food Sci Technol* **54**, 639-649 (2017).

44. S. H. Kim *et al.*, Role of *uvrA* in the growth and survival of *Listeria monocytogenes* under UV radiation and acid and bile stress. *J Food Prot* **69**, 3031-3036 (2006).
45. S. Yildiz *et al.*, Respiratory tissue-associated commensal bacteria offer therapeutic potential against pneumococcal colonization. *Elife* **9** (2020).
46. L. Cao *et al.*, Uncovering the interplay between pH receptors and immune cells: Potential drug targets (Review). *Oncol Rep* **46** (2021).
47. J. A. de la Garza-García *et al.*, Comparative Genome-Wide Transcriptome Analysis of *Brucella suis* and *Brucella microti* Under Acid Stress at pH 4.5: Cold Shock Protein CspA and Dps Are Associated With Acid Resistance of *B. microti*. *Front Microbiol* **12**, 794535 (2021).
48. E. R. Green *et al.*, Bacterial hydrophilins promote pathogen desiccation tolerance. *Cell Host Microbe* **30**, 975-987.e977 (2022).
49. V. R. G. Greffe, J. Michiels, Desiccation-induced cell damage in bacteria and the relevance for inoculant production. *Appl Microbiol Biotechnol* **104**, 3757-3770 (2020).
50. G. Aygün *et al.*, Environmental contamination during a carbapenem-resistant *Acinetobacter baumannii* outbreak in an intensive care unit. *J Hosp Infect* **52**, 259-262 (2002).
51. C. Wendt, B. Dietze, E. Dietz, H. Rüden, Survival of *Acinetobacter baumannii* on dry surfaces. *J Clin Microbiol* **35**, 1394-1397 (1997).
52. B. T. Tierney *et al.*, Multidrug-resistant *Acinetobacter pittii* is adapting to and exhibiting potential succession aboard the International Space Station. *Microbiome* **10**, 210 (2022).
53. S.-Y. Ko *et al.*, *Acinetobacter baumannii* under Acidic Conditions Induces Colistin Resistance through PmrAB Activation and Lipid A Modification. http://dx.doi.org/10.3390/antibiotics12050813.
54. M. D. Adams *et al.*, Resistance to colistin in *Acinetobacter baumannii* associated with mutations in the PmrAB two-component system. *Antimicrob Agents Chemother* **53**, 3628-3634 (2009).
55. T. Rubio *et al.*, Incidence of an Intracellular Multiplication Niche among *Acinetobacter baumannii* Clinical Isolates. *mSystems* **7**, e00488-00421 (2022).
56. G. Sycz *et al.*, Modern *Acinetobacter baumannii* clinical isolates replicate inside spacious vacuoles and egress from macrophages. *PLoS Pathog* **17**, e1009802 (2021).
57. J. S. Distel, G. Di Venanzio, J. J. Mackel, D. A. Rosen, M. F. Feldman, Replicative *Acinetobacter baumannii* strains interfere with phagosomal maturation by modulating the vacuolar pH. *PLoS Pathog* **19**, e1011173 (2023).
58. K. Housh *et al.*, Formation and repair of unavoidable, endogenous interstrand cross-links in cellular DNA. *DNA Repair (Amst)* **98**, 103029 (2021).
59. G. Kapoor, S. Saigal, A. Elongavan, Action and resistance mechanisms of antibiotics: A guide for clinicians. *J Anaesthesiol Clin Pharmacol* **33**, 300-305 (2017).
60. G. V. Mechetin, A. V. Endutkin, E. A. Diatlova, D. O. Zharkov, Inhibitors of DNA Glycosylases as Prospective Drugs. *Int J Mol Sci* **21** (2020).
61. P. Raj *et al.*, Identification of a new and diverse set of *Mycobacterium tuberculosis* uracil-DNA glycosylase (MtUng) inhibitors using structure-based virtual screening: Experimental validation and molecular dynamics studies. *Bioorg Med Chem Lett* **76**, 129008 (2022).
62. R. S. Shapiro, Antimicrobial-induced DNA damage and genomic instability in microbial pathogens. *PLoS Pathog* **11**, e1004678 (2015).
63. E. A. Mullins *et al.*, An HPLC-tandem mass spectrometry method for simultaneous detection of alkylated base excision repair products. *Methods* **64**, 59-66 (2013).
64. A. Asaeda *et al.*, Substrate specificity of human methylpurine DNA N-glycosylase. *Biochemistry* **39**, 1959-1965 (2000).
65. A. Castaño, U. Roy, O. D. Schärer, Preparation of Stable Nitrogen Mustard DNA Interstrand Cross-Link Analogs for Biochemical and Cell Biological Studies. *Methods Enzymol* **591**, 415-431 (2017).

Figures and Tables

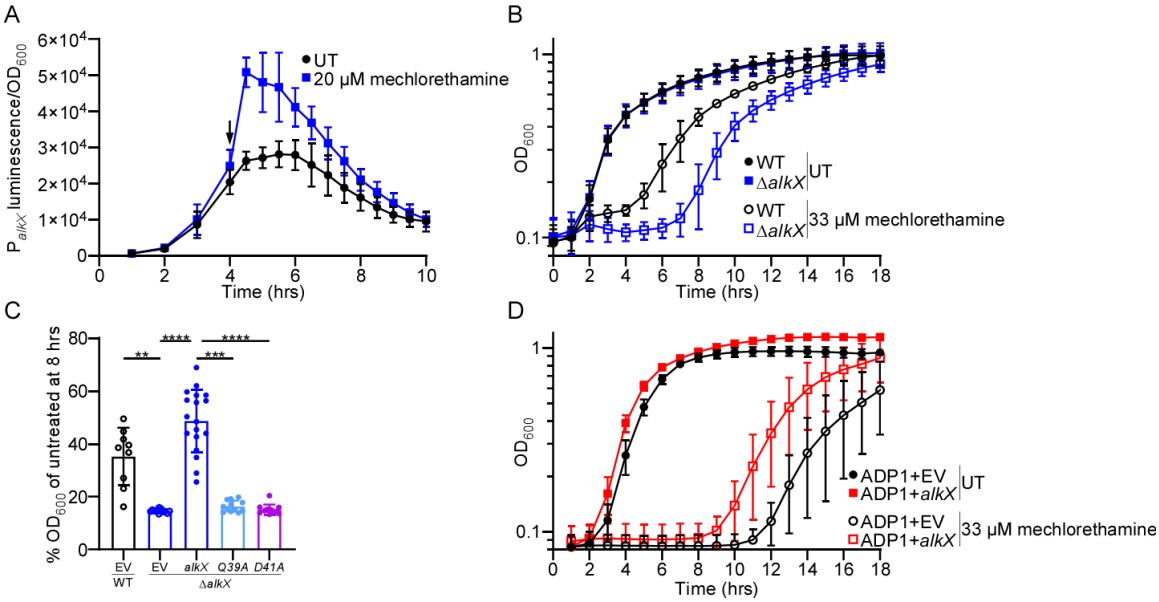

Fig 1. AlkX contributes to DNA alkylation detoxification.
(A) WT *A. baumannii* harboring a P_{alkX}-lux transcriptional reporter fusion plasmid was cultured in LB medium for 4 hr before treatment with 20 μM mechlorethamine or being left untreated (UT). The arrow denotes the timepoint of treatment. Total luminescence and OD_{600} were recorded every 60 min. Data represent the mean ± SD of at least 9 biological replicates performed in technical triplicate. (B) WT or Δ*alkX A. baumannii* strains were cultured in LB medium and left untreated or treated with 33 μM mechlorethamine and OD_{600} was recorded every 60 min. Data represent the mean ± SD of at least 9 biological replicates performed in technical triplicate. (C) WT and Δ*alkX A. baumannii* strain harboring pWH1266 empty vector (EV) or indicated pWH1266-*alkX* expression vectors were cultured in LB ± 33 μM mechlorethamine for 8 hr and OD_{600} was recorded. % OD_{600} was calculated by dividing the OD_{600} values of treated samples by untreated samples. Data represent the mean ± SD, each dot represents an individual biological replicate. ** $p < 0.01$, *** $p < 0.001$, **** $p < 0.0001$ as determined by Dunn's multiple comparisons test. (D) *A. baylyi* ADP1 strains harboring pWH1266 empty vector (EV) or pWH1266-*alkX* expression vectors were cultured in LB medium and left untreated or treated with 33 μM mechlorethamine and OD_{600} was recorded every 60 min. Data represent the mean ± SD of at least 11 biological replicates performed in technical triplicate.

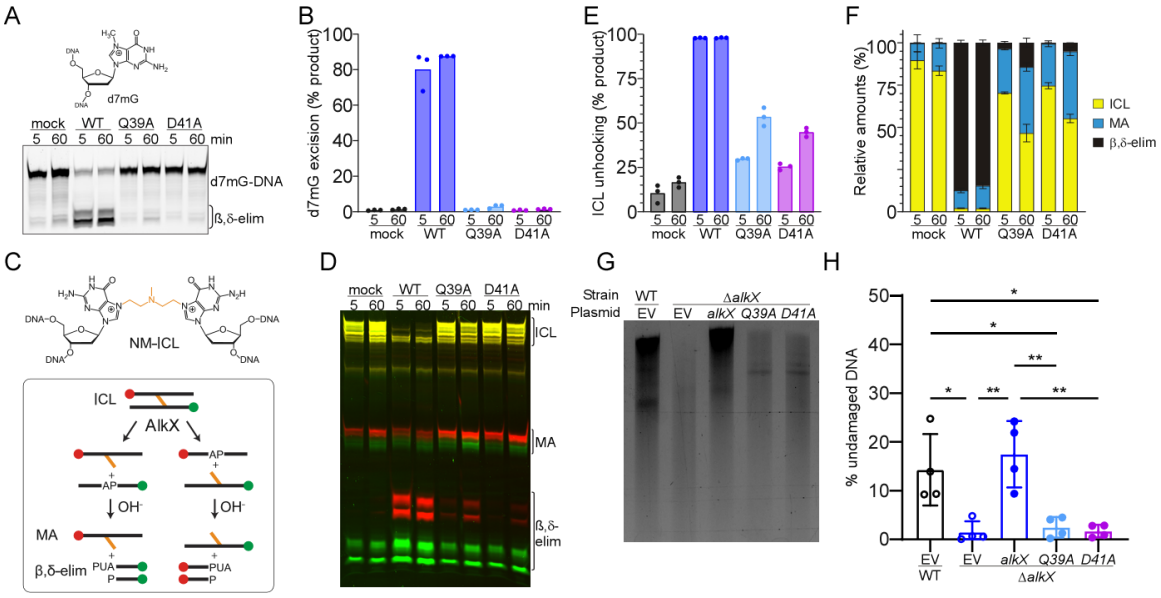

Figure 2. AlkX is an ICL-DNA glycosylase.

(A) AlkX excision of d7mG-DNA, as visualized by denaturing PAGE. Protein was incubated with 5′-Cy5-labeled oligodeoxynucleotide containing a centrally located d7mG substrate for the indicated times, followed by alkali incision of AP site product to generate truncated oligos (β,δ-elim). (B) Quantification of the gel shown in panel A. Data represent the mean ± SD from three independent experiments. (C) Structure of NM-ICL and schematic of the ICL unhooking assay. Red and green circles represent Cy5 and FAM labels. MA, monoadduct; β,δ-elim, β- and δ-elimination products generated from NaOH treatment of AP sites to generate either a 3′-phospho-α,β-unsaturated aldehyde (PUA, β-elimination) or a 3′-phosphate (P, δ-elimination). (D) Denaturing PAGE of NM-ICL and products after treatment with AlkX or buffer (mock) for the indicated times. The image is an overlay of false color Cy5 (red) and FAM (green) fluorescence scans of the gel. (E) Quantification from the Cy5 channel of the gel shown in panel D. Percent product is calculated as ([MA]+[β,δ-elim])/([ICL]+[MA]+[β,δ-elim]). Data represent the mean ± SD from three independent experiments. (F) Relative amounts of ICL, MA, and β,δ-elim from the experiment shown in panel D (mean ± SD, n=3). (G) Representative agarose gel image of WT or Δ*alkX A. baumannii* strains harboring pWH1266 empty vector (EV) or indicated pWH1266-*alkX* expression vectors cultured to mid-log phase then treated with 50 μM mechlorethamine for 1 hr before gDNA was isolated, subjected to BAL-31 digestion, and agarose gel electrophoresis. (H) Percent gDNA undigested was quantified by dividing the intensity of the undigested gDNA band by total lane intensity. Data represent the mean ± SD, each dot represents an individual biological replicate. * $p < 0.05$, ** $p < 0.01$ as determined by Tukey's multiple comparisons test.

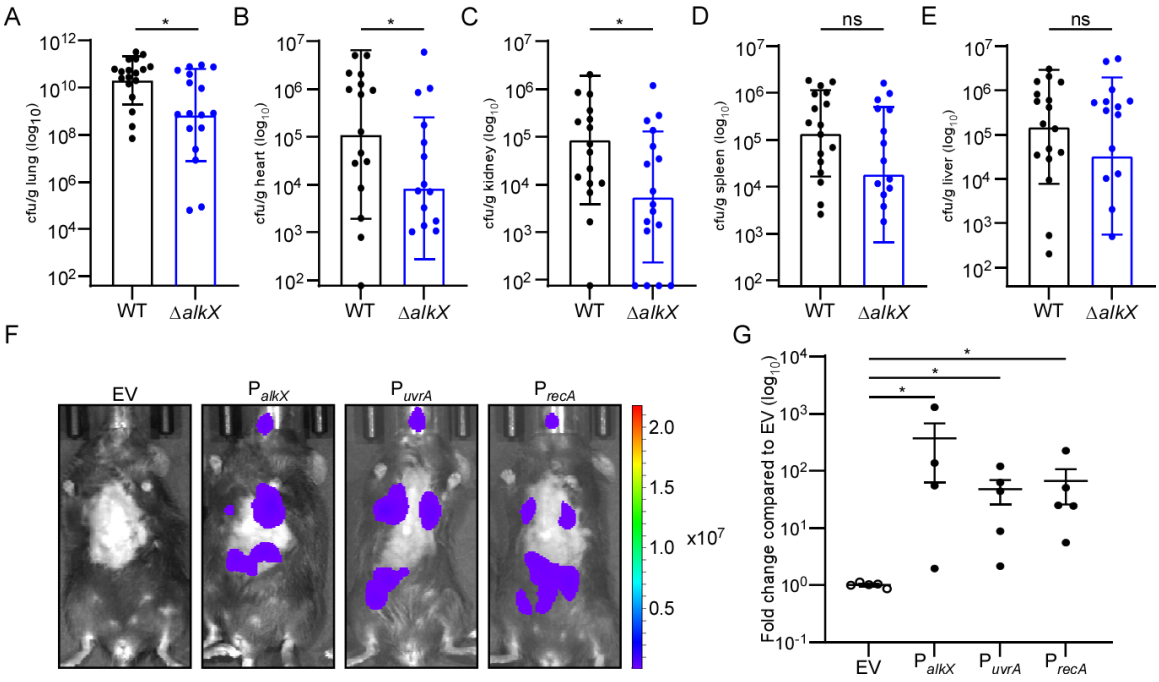

Figure 3. AlkX functions in *A. baumannii* pathogenesis.
(A-E) Female 8-12 wk old C57BL/6J mice were intranasally infected with WT or Δ*alkX A. baumannii*; at 36 hpi mice were sacrificed and organ bacterial burdens in the lungs (A), hearts (B), kidneys (C), spleens (D), and livers (E) were enumerated. Data represent the mean ± SD. Each data point represents one mouse. Y-axis begins at LOD. * $p < .05$ as determined by Mann-Whitney test. (F) Representative *in vivo* bioluminescent imaging 36 hpi of C57BL/6J mice intranasally infected with WT *A. baumannii* strains harboring the indicated luciferase transcriptional fusion reporter plasmids. (G) Fold change of total background-subtracted radiance (p/sec/cm^2/sr) of mice infected with individual transcriptional reporter plasmids, relative to mice infected with empty vector (EV). Data represent the mean ± SEM. Each data point represents one mouse, * $p < .05$ as determined by Dunn's multiple comparisons test.

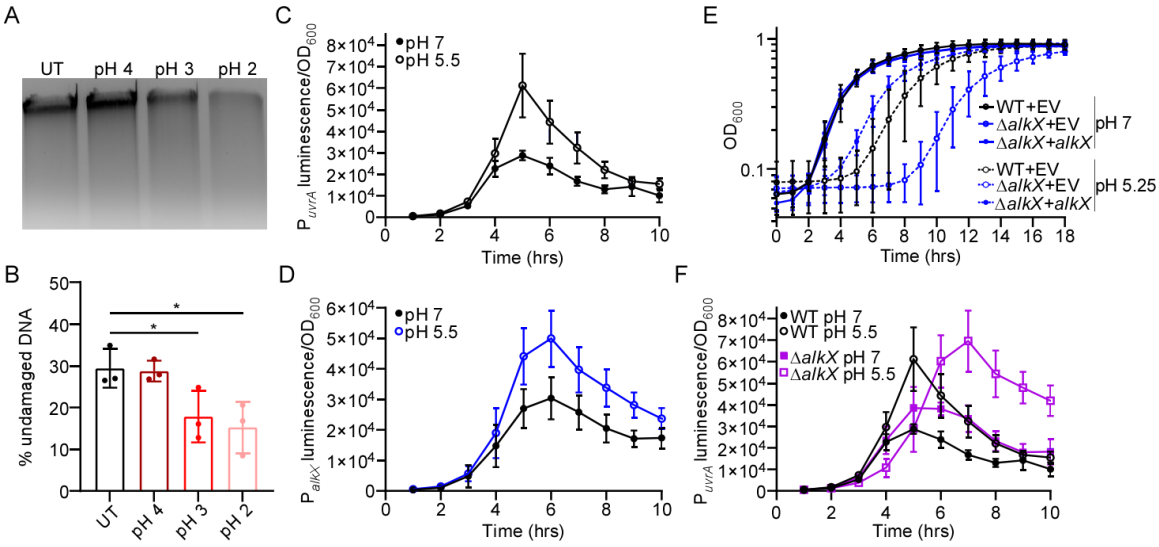

Figure 4. AlkX participates in defense against acidic pH.
(A) Representative agarose gel image of BAL-31 digested *A. baumannii* gDNA collected after 1 hr of culturing at the indicated pH values. (B) Percent of gDNA not digested by BAL-31 quantified from multiple biological replicates. Data represent the mean ± SD, each dot represents an individual biological replicate. UT, untreated. * $p < .05$ as determined by Holm-Šídák's multiple comparisons test. (C,D) WT *A. baumannii* strains harboring either a P_{uvrA}-lux (C) or a P_{alkX}-lux (D) transcriptional reporter fusion plasmids were cultured in LB medium buffered at the indicated pH values. Total luminescence and OD_{600} were recorded every 60 min. Data represent the mean ± SD of at least 9 biological replicates performed in technical triplicate. (E) WT and Δ*alkX A. baumannii* strains harboring pWH1266 empty vector (EV) or a pWH1266-*alkX* complementation vector were cultured in LB medium buffered at the indicated pH values, OD_{600} was recorded every 60 min. Data represent the mean ± SD of at least 6 biological replicates performed in technical triplicate. (F) WT and Δ*alkX A. baumannii* strains harboring a P_{uvrA}-lux transcriptional reporter fusion plasmid were cultured in LB medium buffered at the indicated pH values. Total luminescence and OD_{600} were recorded every 60 min. Data represent the mean ± SD of at least 9 biological replicates performed in technical triplicate.

PNAS

Supporting Information for

An interstrand DNA crosslink glycosylase aids *Acinetobacter baumannii* pathogenesis

Dillon E. Kunkle[1,2,†], Yujuan Cai[3,†], Brandt F. Eichman[3,4], and Eric P. Skaar[1,2,3]

[1] Department of Pathology, Microbiology, and Immunology, Vanderbilt University Medical Center, Nashville, Tennessee, USA

[2] Vanderbilt Institute for Infection, Immunology, and Inflammation, Vanderbilt University Medical Center, Nashville, Tennessee, USA

[3] Department of Biological Sciences, Vanderbilt University, Nashville, Tennessee, USA

[4] Department of Biochemistry, Vanderbilt University, Nashville, Tennessee, USA

[†] These authors contributed equally to this work

*Corresponding authors: Brandt F. Eichman and Eric P. Skaar

Emails: brandt.eichman@vanderbilt.edu and eric.skaar@vumc.org

This PDF file includes:

Figures S1 to S9

Table S1

SI References

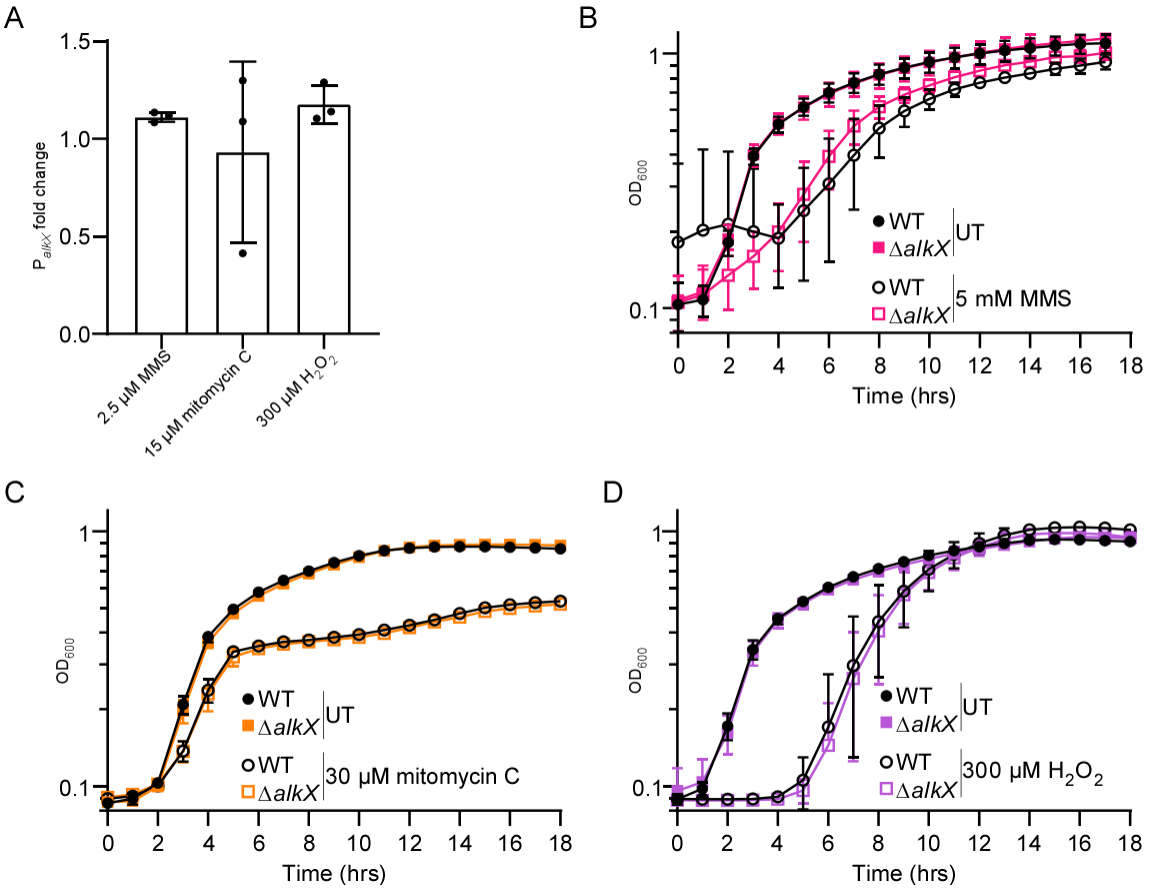

Figure S1. AlkX specifically responds to nitrogen mustard-induced DNA damage.
(A) WT *A. baumannii* harboring a P_{alkX}-lux transcriptional reporter fusion plasmid was cultured in LB medium for 4 hr before treatment with indicated genotoxic agents or being left untreated. One hr post treatment the fold change in luciferase/OD_{600} was calculated relative to untreated cells. Data represent the mean ± SD. Each dot represents an individual biological replicate, measured in technical triplicate. (B-D) WT or Δ*alkX A. baumannii* strains were cultured in LB medium and left untreated (UT) or treated with the genotoxic agents MMS (B), mitomycin C (C), or H_2O_2 (D), and the OD_{600} recorded every 60 min. Data represent the mean ± SD of at least 6 biological replicates performed in technical triplicate.

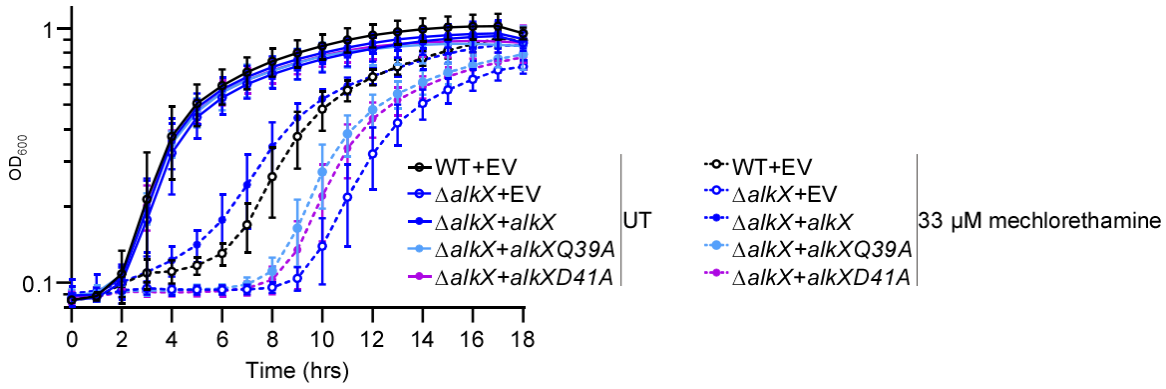

753

754 **Figure S2. AlkX catalytic activity is required for resistance to mechlorethamine-mediated**
755 **killing.**
756 Raw data of *alkX* complementation studies quantified in Figure 1C. WT and Δ*alkX A. baumannii*
757 strains harboring pWH1266 empty vector (EV) or indicated pWH1266-*alkX* expression vectors were
758 cultured in LB ± 33 μM mechlorethamine and OD_{600} was recorded every 60 min. Data represent
759 the mean ± SD of at least 9 biological replicates performed in technical triplicate.
760

761

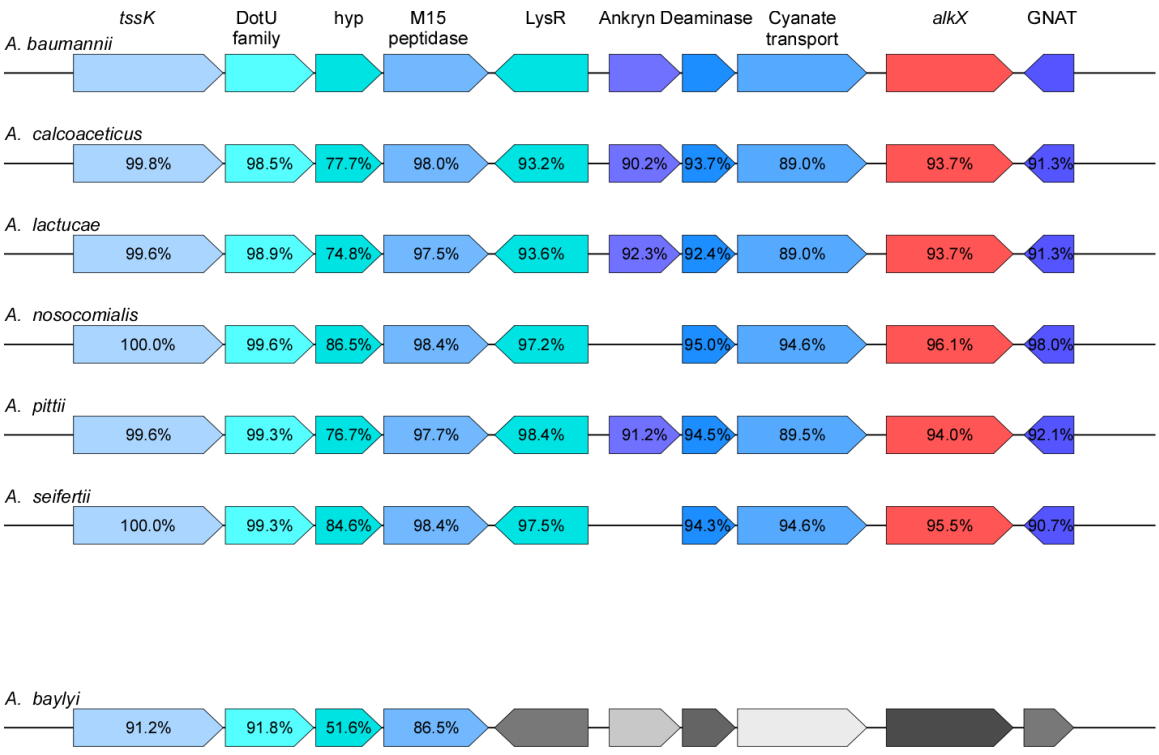

762

763 **Figure S3. Genomic context of *alkX* in *Acinetobacter* species.**
764 Percentages are the overall sequence similarities to the homolog in *A. baumannii*.
765

766

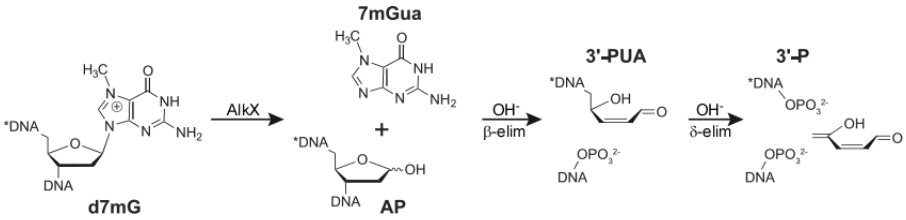

Figure S4. Glycosylase and hydroxide-catalyzed nicking reactions.
The base excision reaction catalyzed by AlkX is shown in the first step, whereby the N-glycosidic bond of N7-methyldeoxyguanosine (d7mG) is hydrolyzed to generate an apurinic/apyrimidinic (AP) site and a free N7-methylguanine (7mGua) nucleobase. The subsequent reactions show the hydroxide catalyzed β- and δ-elimination cleavage of the AP site. Reaction of hydroxide with an AP site generates a polyunsaturated aldehyde at the 3′-end (3′-PUA), which is further cleaved to leave a phosphate on the 3′-end (3′-P).

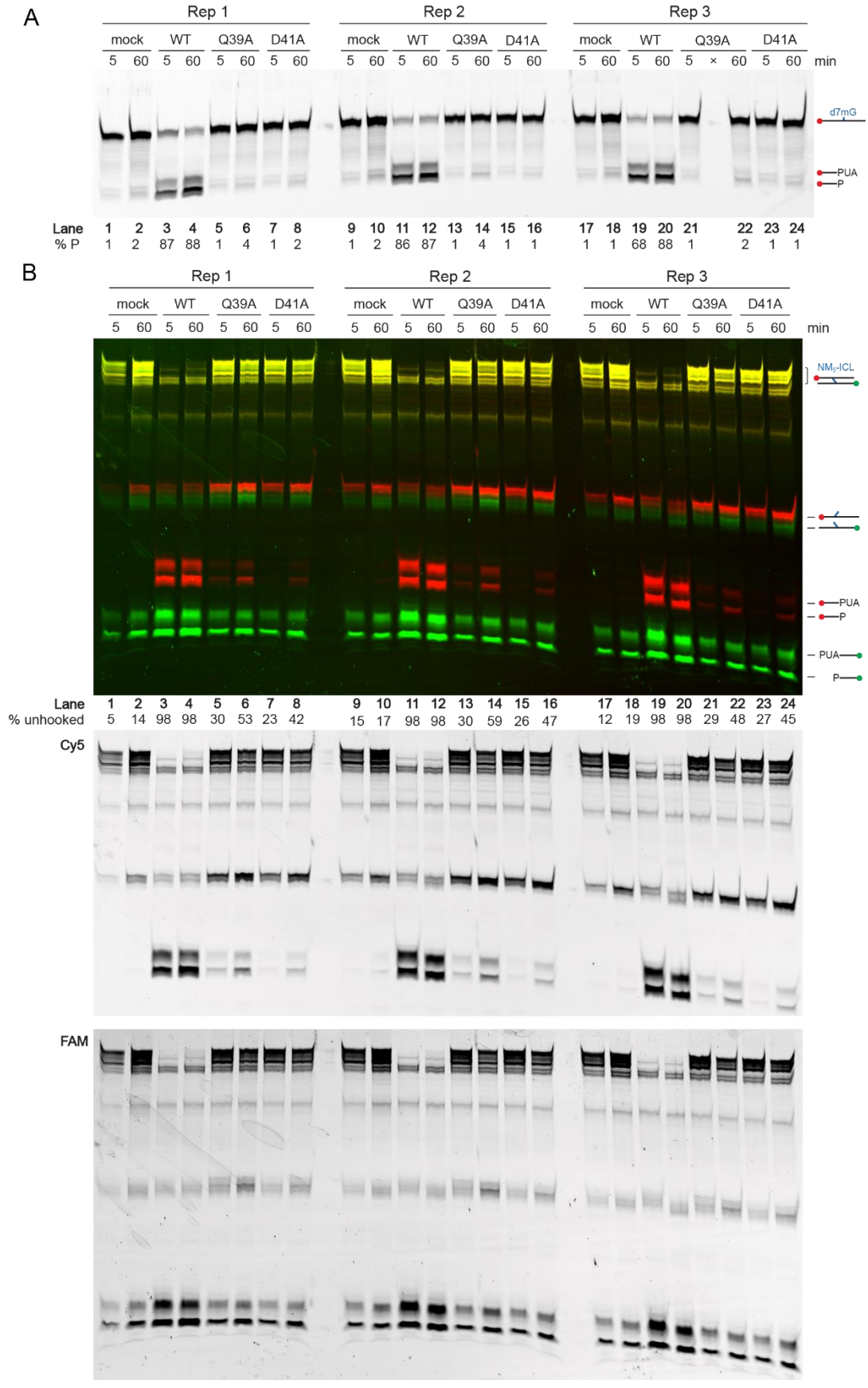
A
Rep 1
Rep 2
Rep 3
mock
WT
Q39A
D41A
5 60
min
d7mG
PUA
P
Lane 1 2 3 4 5 6 7 8 9 10 11 12 13 14 15 16 17 18 19 20 21 22 23 24
% P 1 2 87 88 1 4 1 2 1 2 86 87 1 4 1 1 1 1 68 88 1 2 1 1
B
Rep 1
Rep 2
Rep 3
mock
WT
Q39A
D41A
5 60
min
NM5-ICL
PUA
P
PUA
P
Lane 1 2 3 4 5 6 7 8 9 10 11 12 13 14 15 16 17 18 19 20 21 22 23 24
% unhooked 5 14 98 98 30 53 23 42 15 17 98 98 30 59 26 47 12 19 98 98 29 48 27 45
Cy5
FAM

Figure S5. AlkX DNA glycosylase activity.
Denaturing gels separating substrate and hydroxide-nicked products of AlkX excision assays on d7mG-DNA (A) and NM-ICL (B) substrates shown in Figure 2. Each gel contains three biological replicates. PUA, 3′-phospho-α,β-unsaturated aldehyde (β-elimination); P, 3′-phosphate (δ-elimination). A. Cy5 fluorescent scan of the gel from the d7mG excision assay. B. False-colored overlay (top) of individual Cy5 (middle) and FAM (bottom) fluorescent scans from the NM-ICL unhooking assay. Red, Cy5; green, FAM. Percentage of unhooked ICL was quantified from the Cy5 channel.

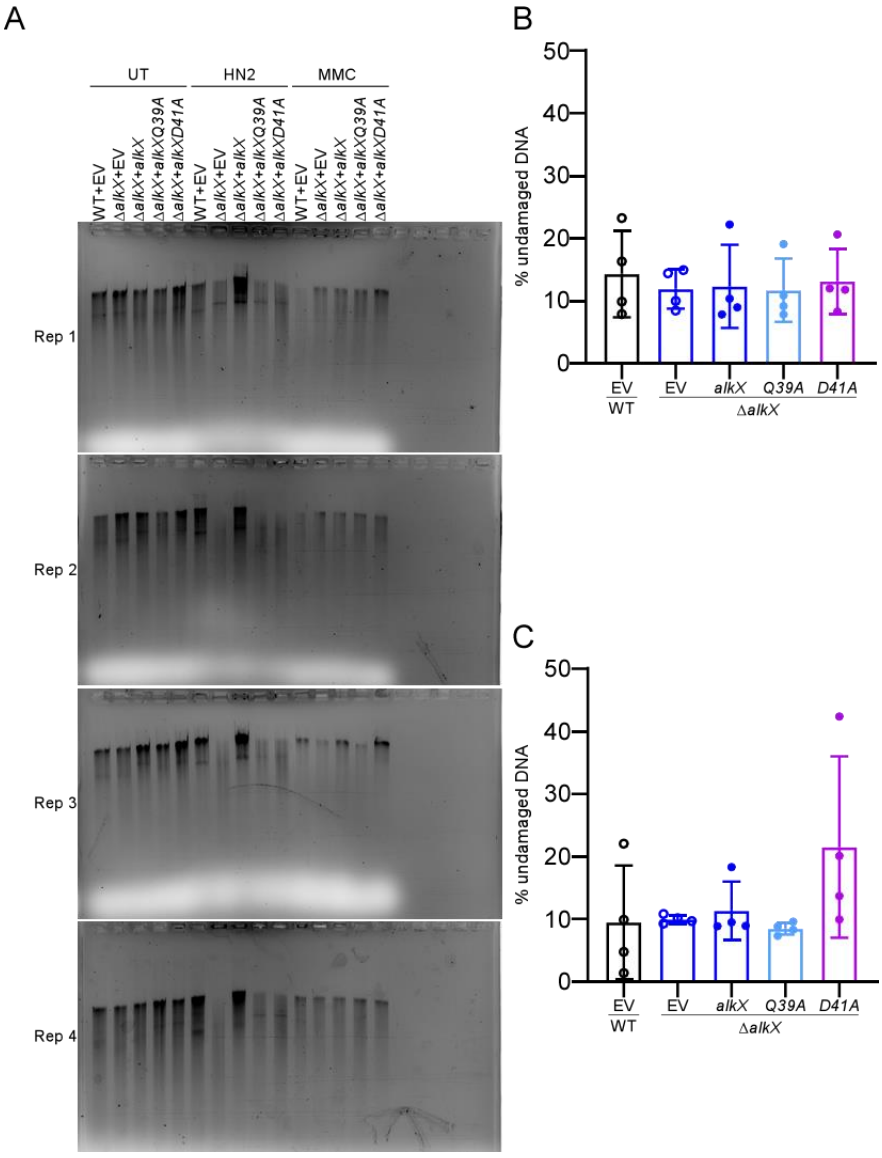

Figure S6. AlkX provides resistance specifically against mechlorethamine-mediated DNA damage.
(A) Raw data of whole-cell DNA damage assays from four biological replicates (rep) quantified in Figure 2H. Agarose gel images of WT or Δ*alkX A. baumannii* strains harboring pWH1266 empty vector (EV) or indicated pWH1266-*alkX* expression vectors cultured to mid-log phase then left untreated (UT) or treated with 50 μM mechlorethamine (HN2) or mitomycin C (MMC) for 1 hr before gDNA was isolated, subjected to BAL-31 digestion, and agarose gel electrophoresis. (B-C) Percent gDNA undigested was quantified by dividing the intensity of the undigested gDNA band by total lane intensity of UT cells (B) or MMC treated cells (C). Data represent the mean ± SD, each dot represents an individual biological replicate.

Strain	% similarity to 17978VU AlkX	First 60 amino acids	
17978VU	-	MTSSLKKIALLKQGLEKNSPFAAGRQGTLEAIEHLGYVQIDTISVVERAHHHILWSRVPD	
19606	99.22	MTSSLKKIALLKQGLGKNSPFAAGRQGTLEAIEHLGYVQIDTISVVERAHHHILWSRVPD	
5075	98.96	MTSSLKKIALLKQGLGKNSPFATGRQGTLEAIEHLGYVQIDTISVVERAHHHILWSRVPD	
AB30	99.48	MTSSLKKIALLKQGLGKNSPFAAGRQGTLEAIEHLGYVQIDTISVVERAHHHILWSRVPN	2010
XH1056	99.22	MTSSLKKIALLKQGLGKNSPFAAGRQGTLEAIEHLGYVQIDTISVVERAHHHILWSRVPD	
UC23022	99.48	MTSSLKKIALLKQGLGKNSPFAAGRQGTLEAIEHLGYVQIDTISVVERAHHHILWSRVPN	
CI107	99.74	MTSSLKKIALLKQGLEKNSPFAAGRQGTLEAIEHLGYVQIDTISVVERAHHHILWSRVPD	
9201	99.48	MTSSLKKIALLKQGLGKNSPFAAGRQGTLEAIEHLGYVQIDTISVVERAHHHILWSRVPN	
AbCTX1	98.70	MTSSLKKIALLKQGLGKNSPFAAGRQGTLEAIEHLGYVQIDTISVVERAHHHILWSRVPN	
AbCAN2	98.70	MTSSLKKIALLKQGLGKNSPFAAGRQGTLEAIEHLGYVQIDTISVVERAHHHILWSRVPN	
5388	99.74	MTSSLKKIALLKQGLGKNSPFAAGRQGTLEAIEHLGYVQIDTISVVERAHHHILWSRVPD	Year isolated
ARC6851	98.96	MTSSLKKIALLKQGLGKNSPFATGRQGTLEAIEHLGYVQIDTISVVERAHHHILWSRVPD	
PA029	100.00	MTSSLKKIALLKQGLEKNSPFAAGRQGTLEAIEHLGYVQIDTISVVERAHHHILWSRVPD	
DT-Ab057	99.74	MTSSLKKIALLKQGLGKNSPFAAGRQGTLEAIEHLGYVQIDTISVVERAHHHILWSRVPD	
DETAB-E51	99.74	MTSSLKKIALLKQGLGKNSPFAAGRQGTLEAIEHLGYVQIDTISVVERAHHHILWSRVPD	
KSK10	98.44	MTSFLKKIALLKQGLGKNSPFAAGRQGTLEAIEHLGYVQIDTISVVERAHHHILWSRVPD	
2021CK-01331	99.74	MTSSLKKIALLKQGLGKNSPFAAGRQGTLEAIEHLGYVQIDTISVVERAHHHILWSRVPD	
2021CK-01407	99.48	MTSSLKKIALLKQGLGKNSPFAAGRQGTLEAIEHLGYVQIDTISVVERAHHHILWSRVPN	
Z198	99.74	MTSSLKKIALLKQGLGKNSPFAAGRQGTLEAIEHLGYVQIDTISVVERAHHHILWSRVPD	2022

Figure S7. Conservation of AlkX in clinical isolates of *A. baumannii*.
Whole genomic sequences of indicated *A. baumannii* clinical isolates were obtained from the NCBI database and searched for the presence of an AlkX homologue. The first 60 amino acids of each protein are shown, with the conserved QxD catalytic domain highlighted in red.

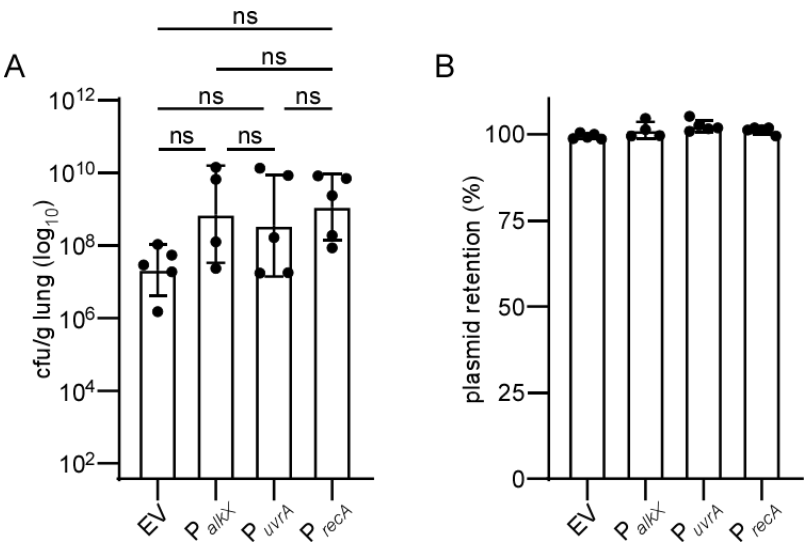

807

808 **Figure S8. Luciferase reporter constructs are well maintained *in vivo.***
809 Data corresponds to *in vivo* imaging data in Figure 3F&G. (A) Bacterial burdens in the lungs at 36
810 hpi of C57BL/6J mice infected with WT *A. baumannii* harboring the indicated transcriptional reporter
811 plasmids. Data represent the mean ± SD. Each data point represents one mouse. Y-axis begins at
812 LOD. ns – not significant as determined by Tukey's multiple comparisons test. (B) Percent retention
813 of WT *A. baumannii* harboring indicated transcriptional reporter plasmids at 36 hpi. Data represent
814 the mean ± SD. Each data point represents one mouse.
815

816

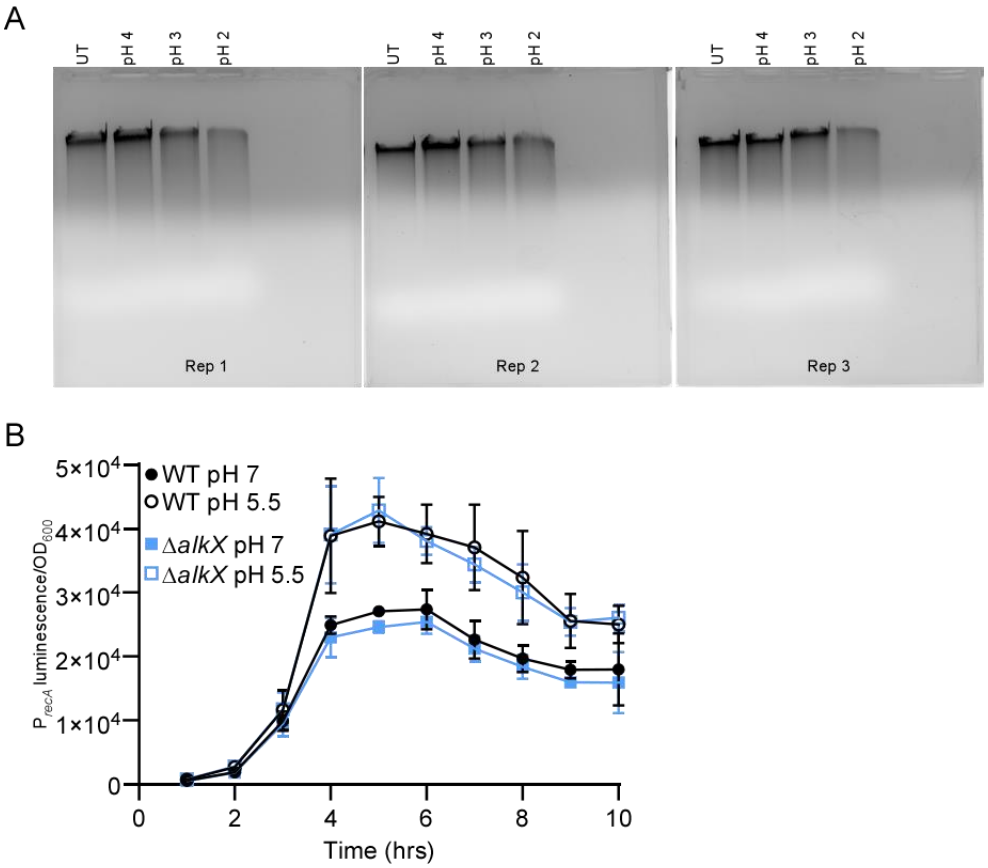

Figure S9. Acidic pH induces DNA damage in *A. baumannii*.
(A) Raw data of whole-cell DNA damage assays from three biological replicates (rep) quantified in Figure 4B. *A. baumannii* gDNA was collected from WT cells after 1 hr of culturing at the indicated pH values and BAL-31 digested. (B) WT or Δ*alkX A. baumannii* strains harboring a P_{recA}-lux transcriptional reporter fusion plasmid were cultured in LB medium buffered at the indicated pH values. Total luminescence and OD_{600} were recorded every 60 min. Data represent the mean ± SD of at least 9 biological replicates performed in technical triplicate.

827 **Table S1. Strains, plasmids, and primers used in this study.**

Strain	**Description**	**Reference**
E. coli DH5α	Plasmid maintenance *E. coli* strain used for all cloning in this study	Lab stock
E. coli HB101	*E. coli* mating strain	Lab stock
A. baumannii 17978VU	Used for WT in this study	Lab stock
A. baumannii Δ*alkX*	17978VU harboring an *ahp* kanamycin cassette insertion into the *alkX* locus	This study
A. baylyi ATCC 33305	Typed ADP1 strain	Lab stock
E. coli Tuner (DE3)	Used for protein expression in this study	Lab stock
Plasmid	**Description**	**Reference**
pWH1266	*Acinetobacter* expression plasmid	(1)
pWH1266-*alkX*	Expression plasmid encoding for *alkX* expression regulated by the native *alkX* promoter	This study
pWH1266-*alkXQ39A*	Plasmid encoding for the expression of a Q39A mutant allele of *alkX*, regulated by the native *alkX* promoter	This study
pWH1266-*alkXD41A*	Plasmid encoding for the expression of a D41A mutant allele of *alkX*, regulated by the native *alkX* promoter	This study
pFLP2	*Acinetobacter* allelic exchange vector	(2)
pUCK1	Template of *aph* kanamycin resistance cassette	
pRK2013	Mating helper plasmid	(3)
pflp2-*alkX-Kan*	Kanamycin marked *alkX* allelic exchange plasmid	This study
pMU368(tet)-lux	Tetracycline marked vector harboring promoterless lux operon *luxABCDE*	(4)
pMU368(tet)-lux-P_{alkX}	*alkX*-lux transcriptional reporter plasmid	This study
pMU368(tet)-lux-P_{recA}	*recA*-lux transcriptional reporter plasmid	This study
pMU368(tet)-lux-P_{uvrA}	*uvrA*-lux transcriptional reporter plasmid	This study
pBG102	pET27 derivative vector with N-terminal 6-his+SUMO tag for protein expression	Vanderbilt University Center for Structural Biology
Primer	**Sequence**	
11575KO_FR1_F_xba	GGTTAAAAAGGATCGATCCTCTAGAGCTAGTGCAATAATTATTGG	
11575KO_FR1_R	TAGTTAGTCAAAAAATCAAATATTGTTGTGTTCATTTAAAAAC	
11575KO_Kan_F	TTTGATTTTTTGACTAACTAGGAGGAATAAATG	
11575KO_Kan_R	AGATTGGTACTCATTATTCCCTCCAGGTAC	
11575KO_FR2_F	GGAATAATGAGTACCAATCTATTTGGGTAG	

11575KO_FR2_R_bam	AAGTTCCTATTCTCTAGGGGGATCCAGATTAGTAAACGTGAAGAATTC	
1266_11575_F_Bam	GCGACCACACCCGTCCTGTGGATCCTAAAGGTTTAGGTGAGTAAAG	
1266_11575_R_Sal	AAGGCTCTCAAGGGCATCGGTCGACTTAAAGCTTGCTGCGAATG	
pWH1266_seq_F	TAGGCTTGGTTATGCCGGTACTG	
pWH1266_seq_R	GGAAGGAGCTGACTGGGTTGA	
pFLP2.seq.F	TGAACGGCAGGTATATGTGATGGG	
pFLP2.seq.F	AAGCGCTCGTTTTCGGAAACG	
11575_ex_F	CGTACAGAGCATGGTTGGAGAACGCAGAGTTG	
11575_ex_R	CCCGATATTCAGTACTGGGACTACAACTGGCG	
NewLong_11575Q39A_F	AGGTTATGTAGCTATTGATACCATATCTGTCGTTGAACG	
NewLong_11575Q39A_R	AAATGTTCAATCGCCTCTAATGTTCCTTGCC	
NewLong_11575D41A_F	TGTACAGATTGCTACCATATCTGTCGTTGAACGTGC	
NewLong_11575D41A_R	ATAACCTAAATGTTCAATCGCCTCTAATGTTCCTTGCC	
pMU368tetLux_p11575_F_sacI	GGACGGCGCGGTACCGAGCTTAAAGGTTTAGGTGAGTAAAG	
pMU368tetLux_p11575_R_Bam	TCCTCTTGCTTCATCTGCAGAAAAATCAAATATTGTTGTGTTCATTTAAAAAC	
recA_lux_F_sac	GGACGGCGCGGTACCGAGCTAAACGTCGAGTTGTGTCG	
recA_lux_R_bam	TCCTCTTGCTTCATCTGCAGCTCAAAAACCTCAATACTCTATG	
uvrA_lux_F_sac	GGACGGCGCGGTACCGAGCTGCATTCATCATAAACAACTATTAG	
uvrA_lux_R_bam	TCCTCTTGCTTCATCTGCAGAAAACATCTCAATTGTGTATTG	
pMU368(tet)lux_seq_F	GCCATACCCGCTCGCTACCCG	
pMU368(tet)lux_seq_R	GATGCTCCAGTAACCATACGG	
Q39A_F	GGGCTACGTGGCGATCGATACCATTAG	
Q39A_R	AGGTGCTCGATTGCTTCC	
D41A_F	CGTGCAGATCGCTACCATTAGCG	
D41A_R	TAGCCCAGGTGCTCGATT	
d7mG_top[a]	Cy5-CACCACTACACC(7mG)ATTCCTTACAAC	
d7mG_bottom	GTTGTAAGGAATCGGTGTAGTGGTG	
ICL_top[a]	Cy5-TTTATTTTTATTTGACTTTTATTTTT[b]	
ICL_bottom[a]	FAM-AAAAATAAAAGTCAAATAAAAATAAA[b]	
[a] FAM, 6-carboxyfluorescein; Cy5, cyanine 5. [b] The underlined G is the site of alkylation		

828

SI References

1. M. Hunger, R. Schmucker, V. Kishan, W. Hillen, Analysis and nucleotide sequence of an origin of DNA replication in *Acinetobacter calcoaceticus* and its use for *Escherichia coli* shuttle plasmids. *Gene* **87**, 45-51 (1990).
2. T. T. Hoang, R. R. Karkhoff-Schweizer, A. J. Kutchma, H. P. Schweizer, A broad-host-range Flp-FRT recombination system for site-specific excision of chromosomally-located DNA sequences: application for isolation of unmarked *Pseudomonas aeruginosa* mutants. *Gene* **212**, 77-86 (1998).
3. D. H. Figurski, D. R. Helinski, Replication of an origin-containing derivative of plasmid RK2 dependent on a plasmid function provided in trans. *Proc Natl Acad Sci U S A* **76**, 1648-1652 (1979).
4. L. J. Juttukonda, W. J. Chazin, E. P. Skaar, *Acinetobacter baumannii* Coordinates Urea Metabolism with Metal Import To Resist Host-Mediated Metal Limitation. *mBio* **7** (2016).